UCRL-ID-152574

IR Extinction Coefficient Measurements of CH and CD GDP Shells

B. Cook, A. Nikroo

March 21, 2003

U.S. Department of Energy
Lawrence Livermore National Laboratory

DISCLAIMER

This work was performed under the auspices of the U. S. Department of Energy by the University of California, Lawrence Livermore National Laboratory under Contract No. W-7405-Eng-48.

Target Area Technologies Program

Mail Station L-481

Ext: 2-3117

March 21, 2003

To: Distribution

From: Bob Cook, Abbas Nikroo

Subject: IR Extinction Coefficient Measurements of CH and CD GDP Shells

Summary

We report wavelength dependent extinction coefficients for both CH and CD glow discharge polymer (GDP) shells. Because these measurements are made on shells opposed to the more ideal coatings made previously on salt plates they represent a more reliable and realistic measure of what can be expected for NIF capsules. The results are listed in Table III on Page 6 for the current wavelengths of interest. For CD the values are similar to what was reported earlier[1] for CD coatings on salt plates. The values for CH are significantly higher than the rough estimate in that report.

Introduction

In a technical memo[1] released near the end of 2001 we reported wavelength dependent extinction coefficients for CH and CD GDP materials determined by depositing films on salt plates and measuring transmission. For CD this was done at a number of thicknesses and thus we had confidence in those results. For CH the results were based on a single 2-μm thick coating and as such represented at best a rough approximation. It is important to note, however, that these measurements represent "ideal" conditions. For a NIF capsule initial deposition will be on a PαMS mandrel which must subsequently be thermally decomposed. Some limited work has indicated that transmission through shells may be worse, and the purpose of the work reported here is to make measurements on shells in order to provide a more realistic evaluation of the relevant wavelength dependent extinction coefficients.

The next section will detail the samples and methods used, and following this the results will be presented. All aspects of the data analysis have been relegated to the Appendix.

Samples and Methods

Shell samples were prepared by coating 2-mm-diameter PαMS shells with either CH or CD and then decomposing the mandrel to leave the GDP shell. For both CH and CD the approach was to start a batch and remove shells at various coating thicknesses so that all the shells would come from a single coating run. In both cases pyrolysis of the PαMS took place after the full thickness was obtained. GDP shell wall thickness was measured after pyrolysis. For the CH shell data an additional sample

---

[1] B. Cook, A. Nikroo, S. Letts, *Measurement of Wavelength Dependent Extinction Coefficients for Target Capsule Materials,* November 7, 2001. Copy available from Bob Cook.

was taken from a different coating run, and in addition several single-wall shards (sh) from a shell from that run were also measured. The wall thicknesses of the shells measured are given in Table I. Note the shell label name includes the *total* transmission thickness of the two walls (excepts CH381sh).

Table I. Shell samples. The first three in each column were from a single coating runs (one CH and one CD). The last two CH samples are from a separate run. Note the label names include twice the wall thickness (decimal point dropped). CH381sh are single wall shards (sh) from a shell from the batch that produced CH778.

CH Shells		CD Shells	
label	wall (μm)	label	wall (μm)
CH246	12.3	CD654	32.7
CH514	25.7	CD912	45.6
CH1108	55.4	CD1162	58.1
CH778	38.9		
CH381sh	38.1		

FTIR transmission measurements were carried out on the CH and CD shells and CH shards from 7000 cm^{-1} to 400 cm^{-1} using a Nicolet Continuum FTIR microscope. The shells were placed on a NaCl disc for measurement. The shell contact spot on the disc was found using the microscope, the microscope was then focused on the shell equator to find the shell midplane, and then the shell was repositioned so that the center of the shell in the x-y plane was at the focal point of the microscope and IR beam. Measurements made by this technique gave transmission values for CH and CD that represented twice the shell wall thickness. To check reproducibility of measurements, the IR spectra were recorded several times for each sample after randomly changing its rotational orientation. In the appendix these results are differentiated by use of an alphabetical suffix on the data label. The measurements on shards were undertaken to see if there was any variation in transmission due to a lensing effect associated with the shells. No evidence of this was seen, however, and the data is simply included in the analysis.

Results

As noted in the Introduction we have relegated most of the data and all of the detailed analysis to the Appendix. In this section we will define terms, indicate the approach, and present the results.

We define the wavelength dependent extinction coefficient, $\varepsilon(\lambda)$, by the expression

$$T(\lambda, t) = T(\lambda, 0)e^{-\varepsilon(\lambda)\cdot t} \tag{1}$$

where $T(\lambda, t)$ is a measurement of the transmission of light of wavelength λ through a sample of thickness t. There are three causes why light intensity in the IR region of the spectrum is attenuated as it passes through a sample. First, there can be reflection out

of the light path due to the material surfaces. Actual losses during transmission come from two sources. First there can be excitation of various vibrational modes in the molecules of the structure, the absorbed energy ultimately dissipated as heat. This is what we are interested in and will determine $\varepsilon(\lambda)$. Second, there can also be internal scattering due to sample density variations. Though these may be problematic for IR layering in some regard, they do not to first order lead to material heating. The degree of this scattering, as well as the surface scattering losses, can be estimated by looking at the degree of transmissive loss in regions of the spectrum where there is no absorption, and using this value a background correction can be made and explicitly included in $T(\lambda,0)$ for each sample.

To determine $\varepsilon(\lambda)$ it is useful to take the natural logarithm of eq 1:

$$\ln T(\lambda,t) = \ln T(\lambda,0) - \varepsilon(\lambda)\cdot t \tag{2}$$

and then define the absorbance, $A(\lambda,t)$, as

$$A(\lambda,t) = -\ln T(\lambda,t) \tag{3}$$

so that eq 1 becomes

$$A_c(\lambda,t) = A(\lambda,t) - A(\lambda,0) = \varepsilon(\lambda)\cdot t.^2 \tag{4}$$

where $A_c(\lambda,t)$ is the absorbance corrected for non-absorptive losses as outlined above. Thus $\varepsilon(\lambda)$ is simply the slope of the $A_c(\lambda,t)$ versus t plot. The challenge of determining $A(\lambda,0)$ for each sample is dealt with in the Appendix.

Although data was collected over the full spectral range from 7000 to 400 cm^{-1}, we will present detailed results only for the 3500 to 2500 cm^{-1} region. The specific wavelengths that have been identified as possibly useful for DT (or D_2) excitation are listed in Table II, and will be specifically identified on plots that in terms of wavenumber rather than wavelength.

CD shells. The analysis of the CD shell data is reasonably straightforward (at least by comparison with the CH shell data!) and these results will be presented first. As noted above three shells were measured, each three independent times. In Figure 1 (same as Figure A-4) we show the baseline corrected absorbance for the CD shells in the wavelength region of interest. The data from the three shells is distinguished by color: green, blue or red. Two different approaches to baseline correction were used and are described in the Appendix. The important point for our discussion here is that the differences in the final results are fairly minor. More important to note is that the three views for each shell *after* baseline correction are very similar - for each shade of

[2] It is perhaps more conventional to define $A(\lambda,t) = -\ln[T(\lambda,t) / T(\lambda,0)]$ so that $A(\lambda,t) = \varepsilon(\lambda)\cdot t$. In doing so one puts the issue of determining the baseline in transmission space, we find it more convenient to work in absorbance space.

Table II. Wavelengths of interest.[3]

λ(μm)	ν(cm^{-1})	excitation
3.139	3186	$Q_1(0,1)D_2+Q_0(1)T_2$
3.161	3164	$Q_1(0,1)D_2+Q_0(1)D_2$
3.190	3135	$Q_1(0,1)D_2+Q_0(1)DT$
3.405	2937	$Q_1(0)DT+S_0(1)T_2$
3.429	2916	$Q_1(0)DT+S_0(0)D_2$
3.464	2887	$Q_1(0)DT+S_0(0)DT$
3.836	2607	$Q_1(0,1)T_2+S_0(0)DT$

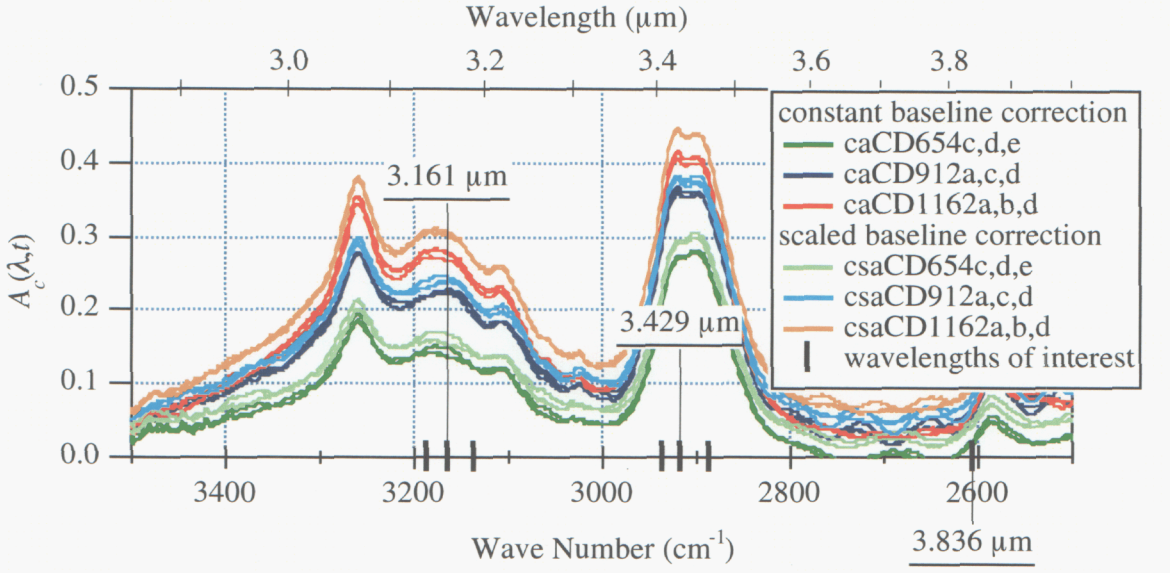

Figure 1. Corrected absorbances using both the constant baseline correction as well as the wavelength dependent correction.

color there are in fact three traces. The view to view reproducibility is excellent which gives confidence in the data.

In Figure 2 (same as Figure A-8) we show the measured extinction coefficients. Things get a little more difficult here, primarily because linear fits of the data at the three thicknesses measured *do not* extrapolate to zero absorbance at wavelengths near 3.429 μm (~2900 cm^{-1} wavenumber). In Figure 2 we show 4 calculations of the frequency dependent extinction coefficient resulting from two methods of baseline correction (constant and frequency dependent) and on two approaches to fitting the thickness dependent absorbance data. The differences because of the baseline correction method are relatively minor and we will not comment further here, the reader is referred to the Appendix for more details. At frequencies *other* than around 2900 cm^{-1} the linear fits of the wavelength dependent absorbance data *do* extrapolate to

[3] Data from P. Clark Souers, *Hydrogen Properties for Fusion Energy*, University of California Press, Berkeley, (1986), p. 330.

near zero absorbance at zero thickness and thus the differences between the blue calculation and the red/orange calculation, where I have forced the fit to pass through the origin, are minor. This is not true around 2900 cm^{-1}. As discussed in the Appendix at some length we believe the problem at 2900 cm^{-1} is related in some fashion to the decomposition of the PαMS mandrel which may be leaving some aliphatic CH absorbing residue on the inside of the shell. Further work will be necessary to better understand this problem and correct it.

In Table III (p 6) we summarize the wavelength dependent results in terms of the range of values taken from Figure 2. What we see is that the values around the 3.161 μm wavelength are only a little higher than the 20 to 23 cm^{-1} values reported for ideal flat samples on salt plates in our previous memo. The values around the 3.429 μm wavelength are perhaps 50% greater than the 22 to 26 cm^{-1} values reported earlier for flat samples. As can be seen in Figure 2 the higher part of the reported range for the current data comes from the forced origin fits. Of particular interest is the evaluation at 3.836 μm, where the value is no more than 10 cm^{-1}, significantly lower than the other wavelengths and in agreement with the flat sample data. More generally the plot in Figure 2 may be useful in selecting an IR excitation wavelength for CD shells that has as yet not been considered.

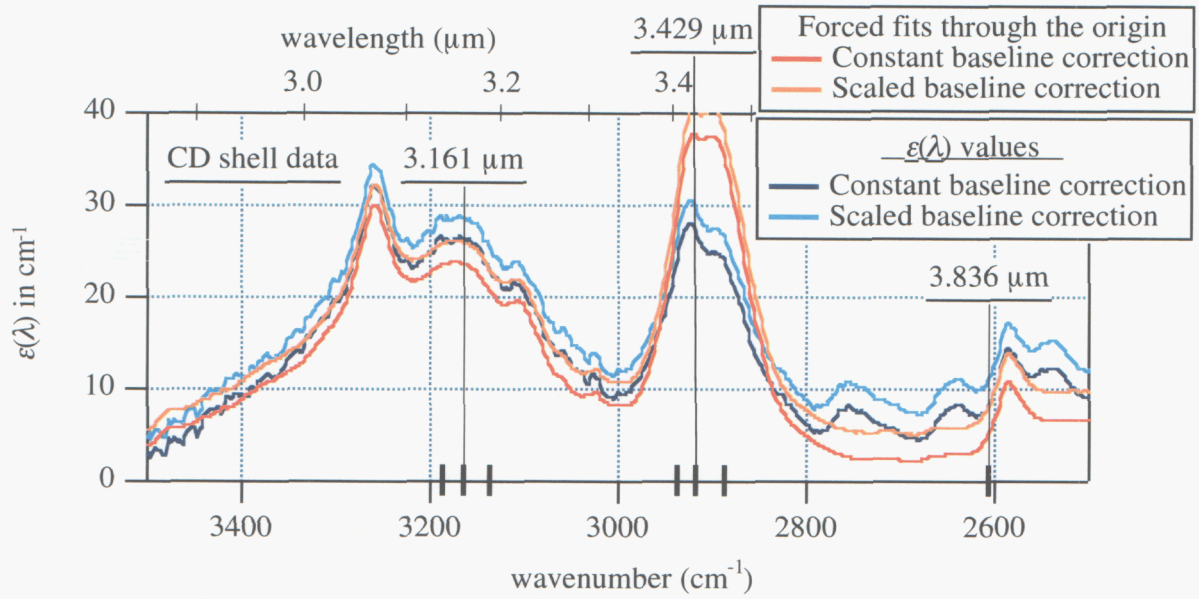

Figure 2. The calculated extinction coefficients. The blue lines are based on simple linear fits of the data with no constraint that the fits include the origin. The red and orange lines are the result if one forces the $A_c(\lambda, t)$ versus thickness plots to pass through the origin.

CH Shells. The absorbances corrected by a constant baseline factor are shown in Figure 3 (same as A-16). The strong absorption at 2900 cm^{-1} is the CH stretch, and it appears that its shoulders may be having some impact in both the 3.2 and 3.8 μm regions. One feature seen here that was not a problem for the CD shells is a strong thin film interference "beating" in some of the spectra, especially bad for the thinnest samples. For the CH246 data this was corrected for by fitting the sinusoidal portion of

the amplitude and subtracting it out. The details are given in the Appendix. It was difficult to do a similar correction for some of the other data sets and thus we used them with only the constant baseline correction. This results in a little scatter in the data for the intermediate thickness samples (see Figure A-19) but it is not a serious problem. As shown in the Appendix the zero thickness intercepts are very nearly zero for the wavelengths of interest, and the quality of the fits as measured by an $<r^2>$ "goodness of fit" parameter is high. Shown in Figure 4 (same as Figure A-20) is a plot of the measured extinction coefficient as a function of wavenumber. Table III (p 6) tabulates the numerical values of the extinction coefficient for both the CH and CD shells, as well as the previously reported numbers for flat salt plate samples. Probably the most important result is that the previously reported CH extinction coefficients, which were estimated from a 2 μm thick layer, were low by at least a factor of two. The current CD results are in line with what was previously reported for flats, though there is still an unresolved problem around 3.4 μm as mentioned above.

The results show that if one wants to use a wavelength around 3.2 μm that perhaps CH is a little better but there really is little difference between the two materials. There seems to be no advantage of using CD shells at 3.4 μm instead of CH or CD shells at 3.2 μm unless the 3.4 μm light is more strongly absorbed by the DT. We also note that measurements for vapor deposited normal polyimide around 3.4 μm likewise give extinction coefficients in the mid 20 cm^{-1} range.[4] Clearly the 3.8 μm wavelength should be reexamined with respect to its DT absorbance since for the shell data presented here it offers the most transmission if CD shells are used. Plans for a direct measure of the frequency dependent IR absorbance of DT are being developed by the cryo group for this spring, and those results coupled with what we report here should make it clear what the best wavelength and shell material[5] are for IR enhanced layering.

Table III. Summary of wavelength dependent extinction coefficients, $\varepsilon(\lambda)$, in units of cm^{-1}.

	shells(this work)		flats(Nov, 2001)[6]	
λ	CD	CH	CD	CH
3.139	23-29	19	23	11
3.161	23-29	22	23	10
3.190	22-25	21	20	7
3.405	24-33	-	22	1220
3.429	26-40	-	26	1210
3.464	24-38	-	23	720
3.836	5-11	36	7*	7*

* - Not reported in the November 2001 memo but calculated from that data set.

[4] M. Anthamatten, S. Letts, and R. Cook, *FTIR Characterization of Vapor Deposited & Solution Cast Polyimide*, February 12, 2002, copy available from Bob Cook.

[5] Data on fully deuterated vapor deposited polyimide is now being collected and will be released in the near future to complement the data previously released for normal vapor deposited polyimide (previous footnote).

[6] see footnote 1 on page 1

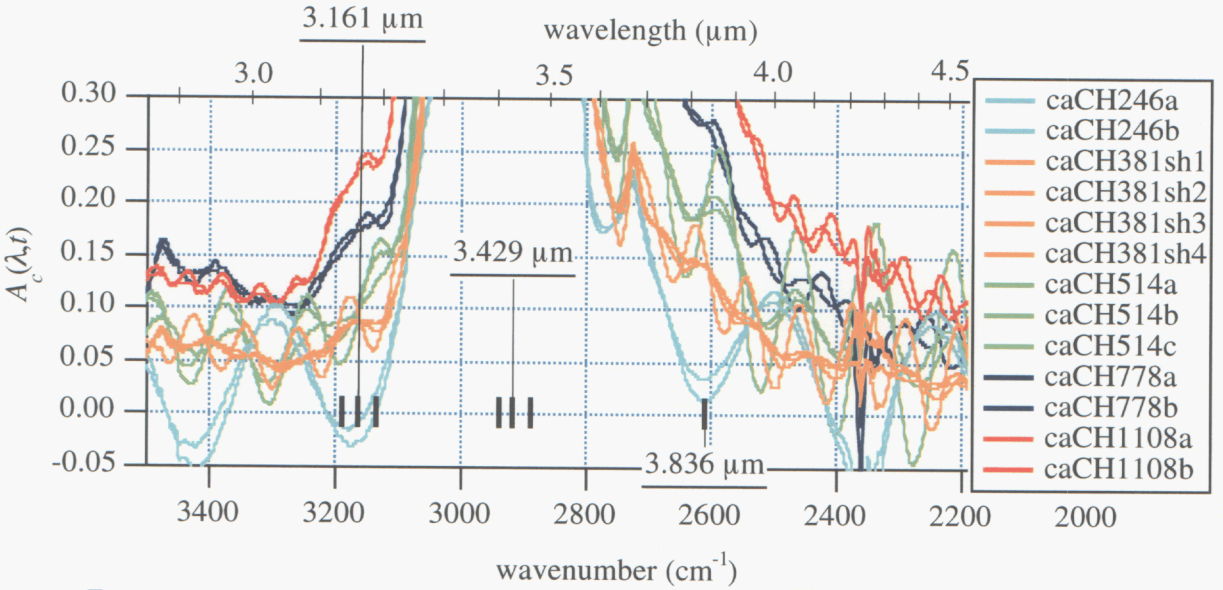

Figure 3. Absorbances corrected by constant baseline correction $\langle A \rangle$.

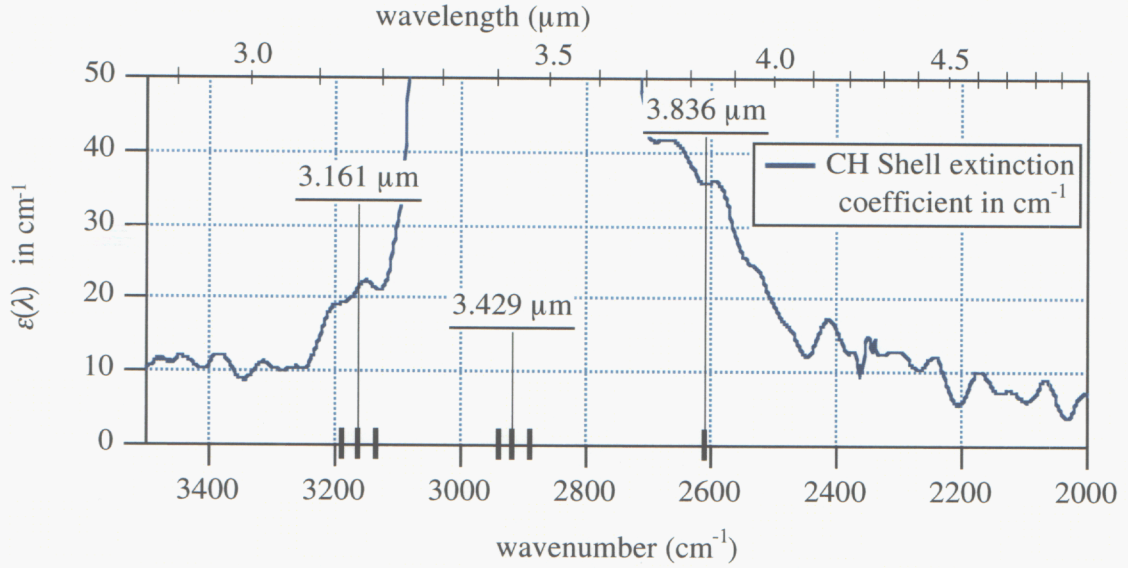

Figure 4. CH shell extinction coefficient (cm^{-1}) as a function of wavenumber.

Appendix

Our approach here will be to present the data and go through the complete analysis in somewhat gory detail, in part because there are some ambiguities, and impart simply to create a record of what was done. The general approach will be similar to what we did in the original study,[7] and additional details may be found there. We'll start with the CD data since it is somewhat cleaner.

[7] see footnote 1 on page 1

CD Shells

As shown in Table I three CD shell thicknesses were measured, and for each thickness three sets of data were obtained by collecting three independent spectra from each shell (*i.e.* spectra obtained after reorienting the shell). The raw transmission data is shown in Figure A-1 over the range of 7000 to 400 cm^{-1}. From this data the raw absorbance data is obtained from eq 3 with the transmittance T being expressed as a decimal. This uncorrected absorbance data is displayed in Figure A-2.

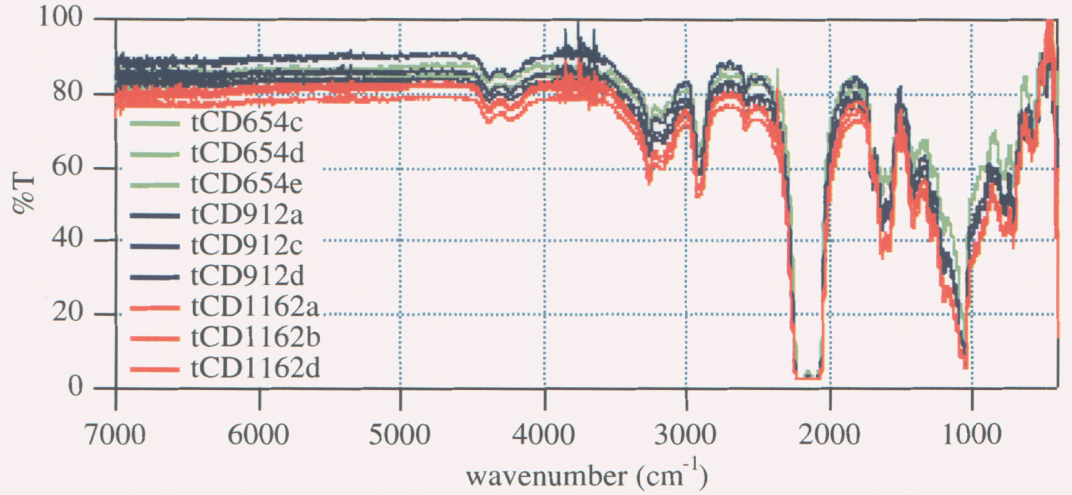

Figure A-1. Transmission data for CD shells. Three shells were measured, the suffixes distinguish the 3 independent spectra obtained from each shell. The prefix "t" means transmission.

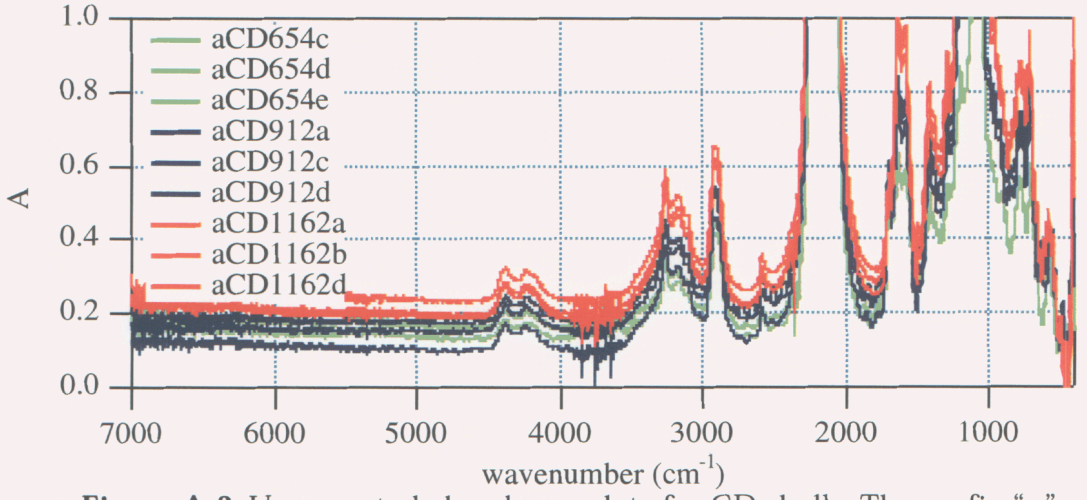

Figure A-2. Uncorrected absorbance data for CD shells. The prefix "a" means absorbance.

The next problem is to determine the baseline correction for each data set. It is clear from the intensities above 4500 cm^{-1} that each data set has its own baseline correction. Two approaches were taken. The first is similar to what was done

previously - the average A in a region where there was no vibrational absorption was used. For this data I selected 5200 to 4600 cm^{-1} to obtain this average. Using this approach one determines the $A(\lambda,0)$ values shown in the first column of Table A-I. Note that in this approach the background correction in fact has no wavelength dependence. An alternative approach is suggested by a more careful look at Figure A-2. It appears that the absorbance between 7000 and 4500 cm^{-1} is quite linear and slightly tilted downward from left to right in the figure. This suggests that there may be a weak wavelength dependence to the background. To test this idea I did a linear fit of the uncorrected absorbance as a function of wavenumber ($\bar{\nu}$) from 7000 to 4600 cm^{-1}, letting

$$A(\lambda,t) = m\cdot\bar{\nu} + b\ . \qquad \text{(A-1)}$$

The fitted values of m and b for each data set are shown in Table A-I. An illustration of the fit for the data is shown in Figure A-3. With these fitted backgrounds we now have a true "wavelength dependent" $A(\lambda,0)$.

Table A-I. CD data background correction parameters. The column labeled $A(\lambda,0)$ is the average value between 5200 and 4600 cm^{-1}. The columns labeled m and b are the fitted parameters from eq A-1 for the data from 7000 to 4600 cm^{-1}.

data set	$A(\lambda,0)$	m	b
aCD654c	0.1672	1.068×10^{-5}	0.1167
aCD654d	0.1357	1.229×10^{-5}	0.0769
aCD654e	0.1649	1.084×10^{-5}	0.1140
aCD912a	0.1015	1.212×10^{-5}	0.0412
aCD912c	0.1512	0.654×10^{-5}	0.1185
aCD912d	0.1764	0.700×10^{-5}	0.1415
aCD1162a	0.2368	1.522×10^{-5}	0.1610
aCD1162b	0.1915	1.765×10^{-5}	0.1024
aCD1162d	0.2000	1.508×10^{-5}	0.1247

It turns out that the differences between these two approaches are quite minor. In Figure A-4 I show the corrected absorbances in the region of interest (the specific wavelengths of interest are marked) using both approaches, the differences are quite small. The wavelength dependent extinction coefficient can be calculated from this data by plotting the absorbance at a specific wavelength as a function of sample thickness and determining the slope (eq 4). These plots for the constant baseline correction are shown in Figure A-5, where I have extended the linear fit of the data to zero thickness. A troublesome aspect of these fits is that the zero thickness intercept is non-zero, and especially bad for the 3.4 μm wavelengths. More on this momentarily. In Figure A-6 I show the extinction coefficient (in units of cm^{-1} rather than μm^{-1}) as a function of wavenumber for both the constant and linear baseline correction data. This data was obtained by doing linear fits at *every* wavenumber point in the spectrum. Figure A-7 shows the zero thickness intercept (b, eq A-1) as a function of wavenumber.

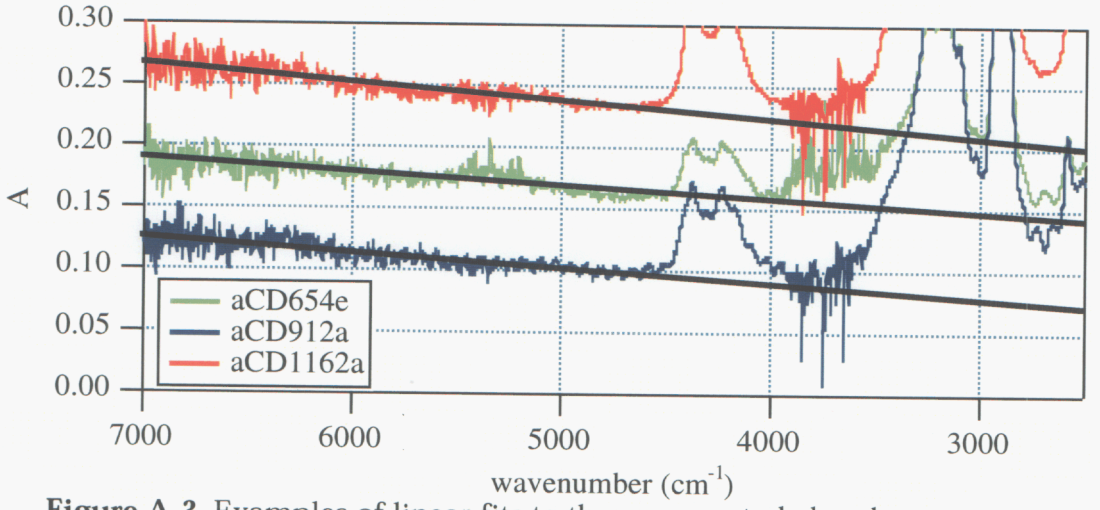

Figure A-3. Examples of linear fits to the uncorrected absorbance.

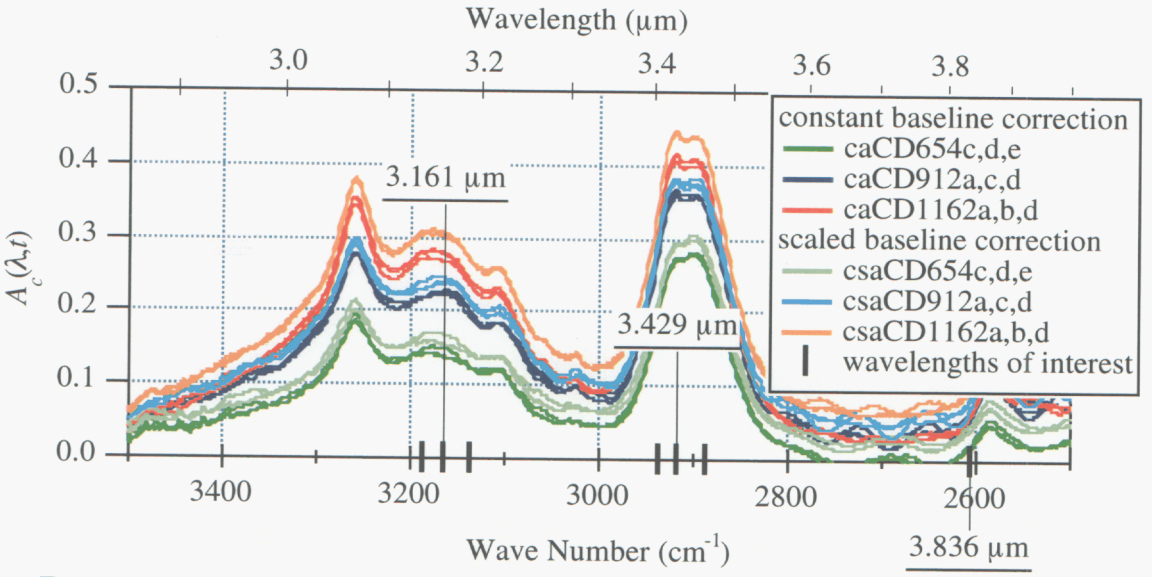

Figure A-4. Corrected absorbances using both the constant baseline correction as well as the wavelength dependent correction.

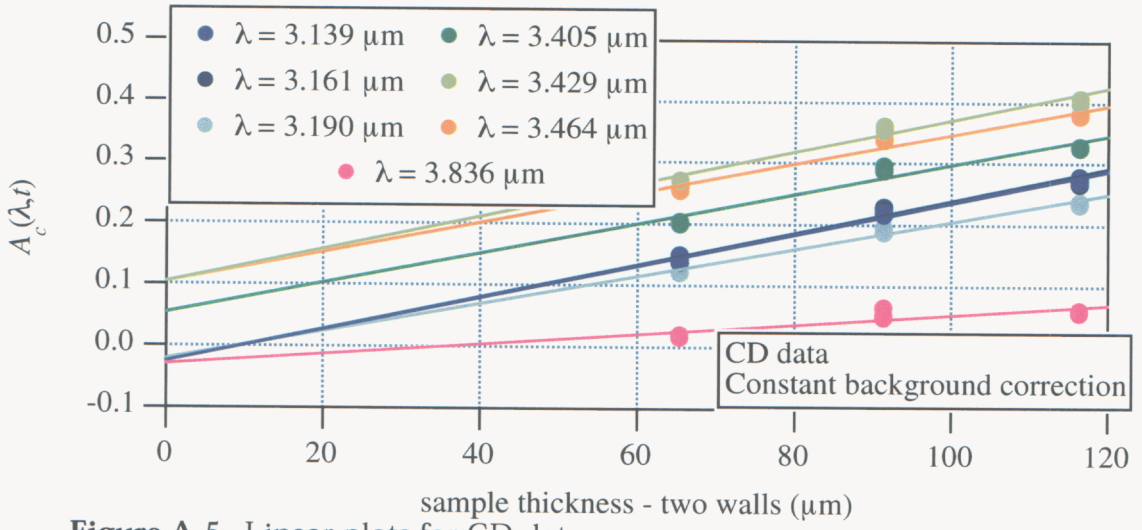

Figure A-5. Linear plots for CD data.

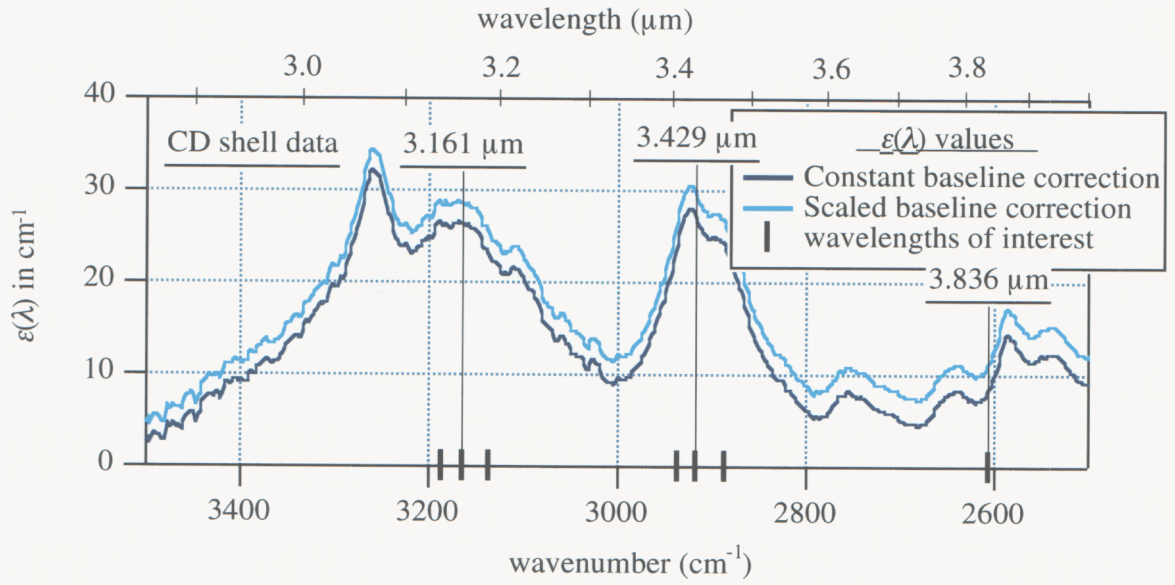

Figure A-6. Extinction coefficient in cm^{-1} as a function of wavenumber.

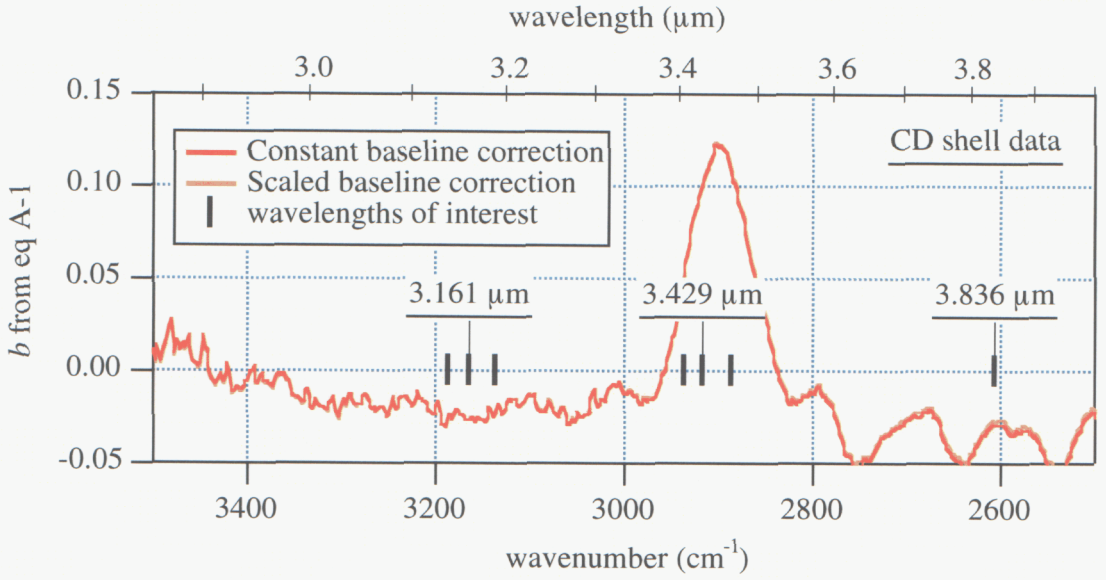

Figure A-7. Value of linear intercept *b* (eq A-1).

The problem of non-zero intercept at zero sample thickness is problematic. One manifestation of the problem is that the measured extinction coefficients around 3.1 and 3.4 μm are about the same, 25 to 30 cm^{-1}, in contrast to what one might initially expect by simply looking at the baseline corrected absorbance in Figure A-4. Here it certainly looks like there is more absorbance around 3.4 μm than 3.1 μm. If we *force* the plots of $A_c(\lambda, t)$ versus thickness to pass through the origin by fitting to $A_c(\lambda, t) = \varepsilon(\lambda) \cdot t$ we find that the extinction coefficients increase around 3.4 μm while decreasing somewhat at 3.1 and 3.8 μm as one would expect by twisting the lines in Figure A-5. In Figure A-8 I show the values of the extinction coefficient evaluated in this manner over the range from 3500 to 2500 cm^{-1} and in Figure A-9 I show for comparison the quality of the linear fits if one does this. Remember that there are three data points at each thickness, their agreement indicated by their near perfect overlap gives confidence that the failure of the normally fitted line to pass through the origin is not due to random data scatter.

The unusual appearance of the plot of intercept *b* in Figure A-7 suggests another explanation. The position of the peak centered at about 2900 cm^{-1} corresponds closely with the aliphatic CH stretch. One interpretation is that all coatings regardless of thickness have an added constant aliphatic CH contribution. How might this occur? One possibility is that this is related to the pyrolysis of the PαMS mandrel. This effect has been seen before and was reported briefly in the FY02 2nd and 3rd Quarter ICF Program progress reports.[8] We repeat the highlights here.

[8] *Inertial Confinement Fusion Program Progress Report*, FY02 2nd Quarter, pp 44-46; FY02 3rd Quarter, pp 41-42.

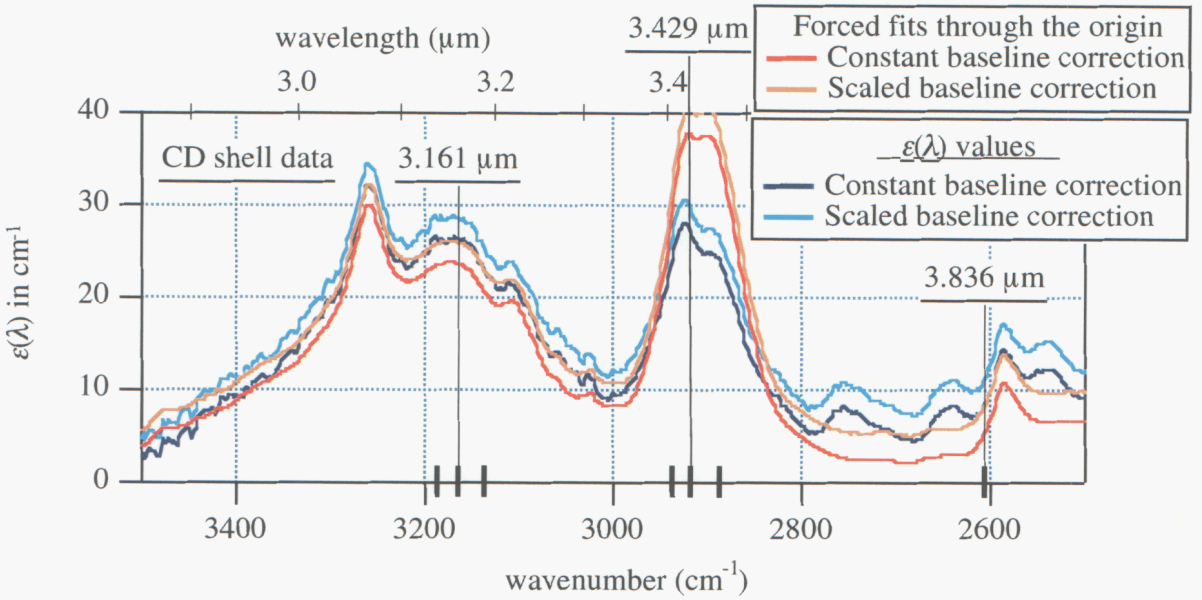

Figure A-8. The calculated extinction coefficients if one forces the $A_c(\lambda, t)$ versus thickness plots to pass through the origin

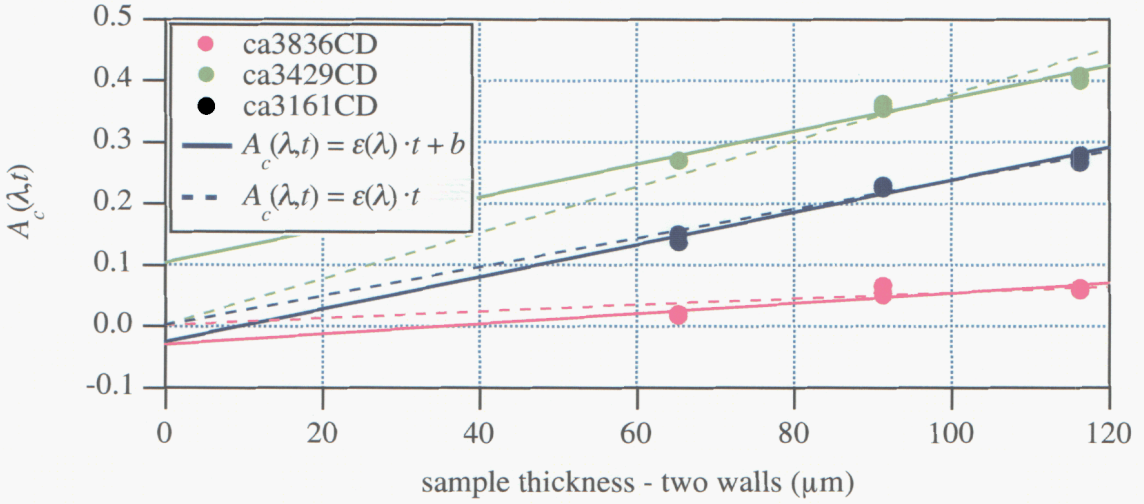

Figure A-9. Comparison of simple linear fit and forced fit through the origin.

The basic observation that early on motivated concern was that transmission through CD shells at 2900 cm^{-1} was reduced relative to flat coatings on salt plates, suggesting that PαMS and/or the pyrolysis were responsible in some way. Our first thought was that some fraction of the αMS monomer was being trapped in the CD shell wall while diffusing out. Since the monomer is hydrogenated it should contribute to the 2900 cm^{-1} absorption. To test this PαMS mandrels were coated with CD, and then several were cut in half to make hemishells. These hemis were then pyrolyzed along with intact shells, and IR spectra were then obtained through single walls of both

the hemi and intact shells. The expectation was that since the αMS would not need to diffuse through the hemis they would have reduced 2900 cm^{-1} absorption relative to the intact shells. The results shown in Figure A-10 were surprising, but certainly indicated that trapped αMS because of diffusion through the shell wall was not playing a role. In fact the absorbance for the hemishell sample was 30% higher at 2900 cm^{-1}.

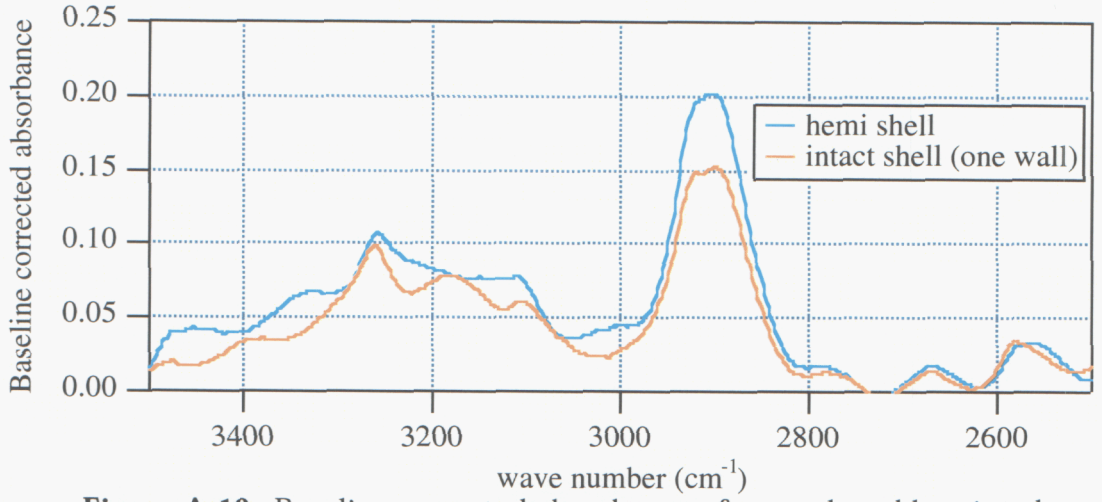

Figure A-10. Baseline corrected absorbance of a pyrolyzed hemi and intact CD shell.

A second experiment to explore this issue was performed. If this enhanced 2900 cm^{-1} absorption is related to the mandrel then one would expect that it would be independent of shell thickness, which is basically the result we see in the current data. In an earlier experiment the effect was examined as follows. PαMS mandrels were coated with CD for 24 h and 96 h, representing coatings of about 10 and 40 μm. Both batches were pyrolyzed and the IR spectra obtained through a single wall. In Figure A-11 we show the baseline corrected absorbance measurements for each sample, and for comparison purposes have multiplied the 96-h results by 25%. Clearly we see that the thinner coating has a higher net "concentration" of CH stretch absorbing structures.

One explanation of these results is that the PαMS mandrel leaves behind some level of residue that absorbs strongly at 2900 cm^{-1}, and the amount of this residue depends only on the original PαMS shell and/or pyrolysis conditions. There has been some evidence in the past of a visible residue left after pyrolysis in some runs, but it has always appears very diaphanous when seen and seemed unlikely to have any significant thickness. However there may be more there than we are seeing and a further investigation is warranted.

Since we have this older data for 10 and 40 μm walled shells it is interesting to see how it compares with the current set of data. We did not initially include it since the coating conditions were at the very least separated in time from the current study, and the shell wall thickness was only estimated based on the coating rate. However in Figure A-12 we add this data to the data in Figure A-9 to see if it sheds light on the linearity calculation. What we see is that this older data tends to support the forced fit (dashed line) interpretation. I don't quite know what to make of this since I think it

adds to the confusion rather than reducing it. What I think we can say is that we have reasonably well bracketed the range of the wavelength dependent extinction coefficient by the various fitting approaches. The results are summarized in Table III in the main section of the memo.

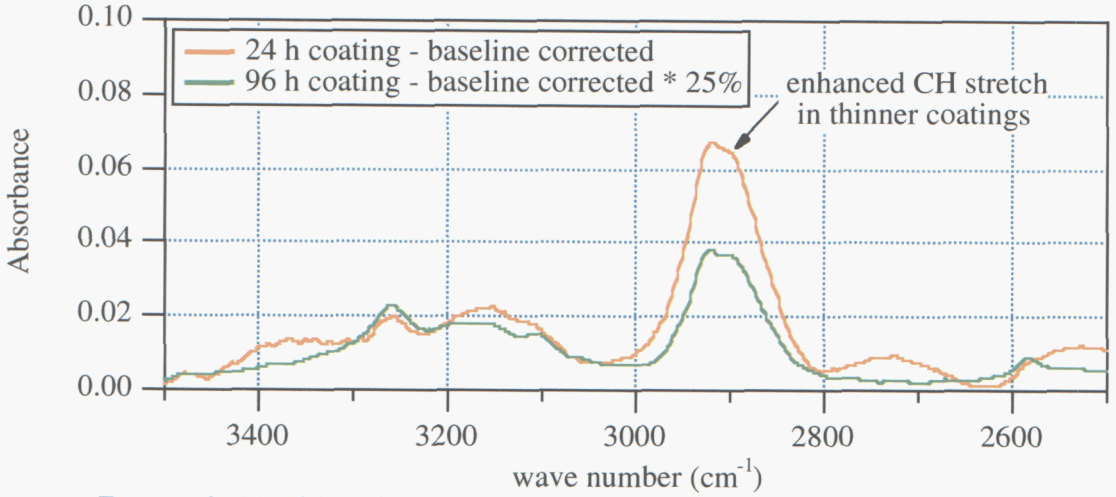

Figure A-11. Absorbance measurements from two shells, one with 4 times as much CD coating. For comparison the absorbance of the thicker shell has been multiplied by 25% to show that the net "concentration" of CH stretch absorbing structures is higher in the thinner coating.

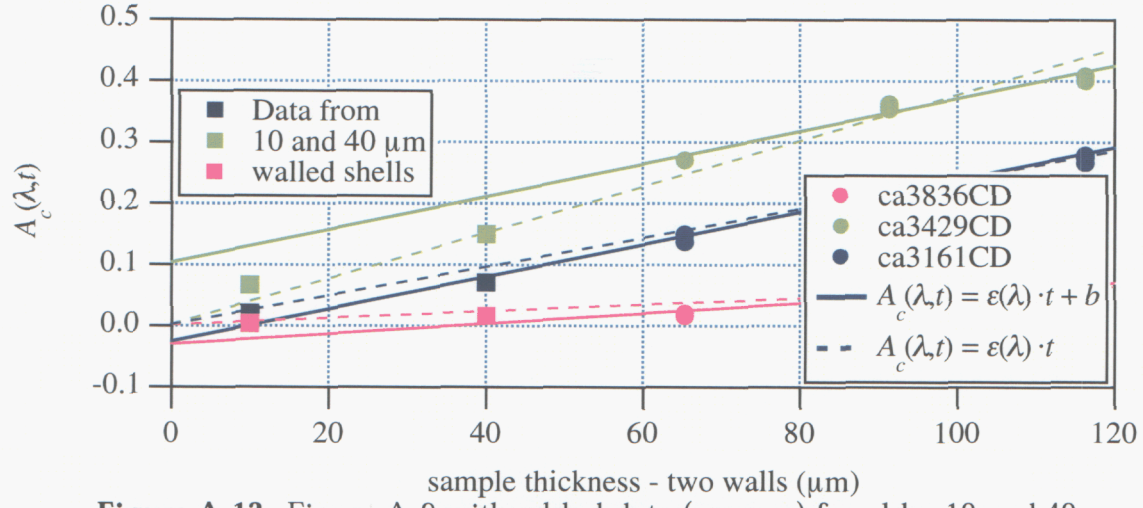

Figure A-12. Figure A-9 with added data (squares) for older 10 and 40 mm thick shells. For this data transmission is only through a single wall.

In closing this section let me add one last note. If there is a thin level of CH absorber on the inner shell wall this means that a disproportionate amount of the heat generation from IR illumination would occur at the ice/wall interface. It is not clear to me whether this is better or worse than uniform heat generation, but presumably it is a problem that can be easily modeled.

CH Shells.

The CH data is a little more complicated to deal with, but lets proceed. Four shell thicknesses (intact shell - double wall) were measured, as well as single wall measurements made on shards from one shell run. The shell "names" are given in Table I. In Figure A-13 we show the raw transmission data for all 13 samples. One can make several observations. First, there is much less background loss in the single wall shard data than for the shells. For example the transmission through the CH246 shell with a total of 24.6 μm of wall is less than through the 38.1 μm thick shard. This is probably due to scattering losses associated with spectra through two walls. Second, the background contribution can vary significantly for different spectra from the same shell. Remember that the green, blue (light and dark), and red spectra come from the same four shells, the multiple data being simply different mountings of the shell in the spectrometer. Third, some of the spectra of the thinner samples (especially CH246) have significant waviness due to thin wall interference effects. It clearly is sample (or sample orientation) dependent, however, since even one of the CH514 spectra exhibits significant beating. Thus it is clear that background correction and data extraction will need to be done with care.

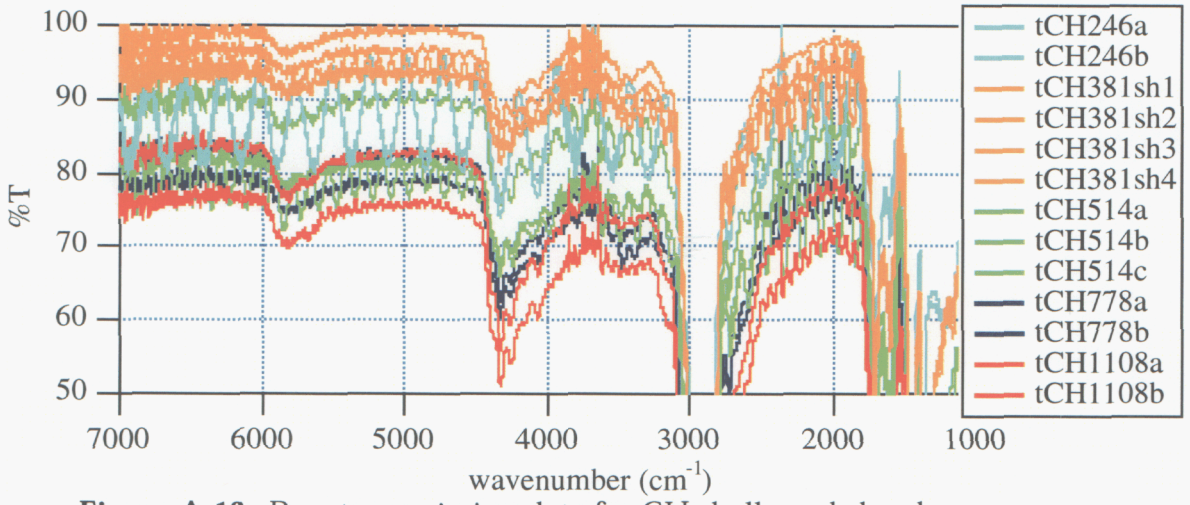

Figure A-13. Raw transmission data for CH shells and shards.

In Figure A-14 we convert the %T data to uncorrected absorbance data, $A = -\ln(\%T/100)$. Determining the baseline correction is more challenging here in part because of the strong CH stretch overtone at 5800 cm^{-1} that was absent in the CD data. However like with the CD data we will estimate a constant baseline correction by determining the average value of the absorbance over the relatively flat region from 5250 to 4750 cm^{-1}. Because the absorbance of some of the samples exhibits significant thin film beating I'll calculate these average values by fitting the absorbance in the 5250 to 4750 cm^{-1} region with

$$A = \langle A \rangle + c_0 \sin(c_1 \bar{\nu} + c_2) \qquad \text{(A-2)}$$

where $\bar{\nu}$ is the wave number. The uncorrected absorbance in the 5250 to 4750 cm^{-1} region with overlaid fits in black is shown in Figure A-15. Table A-II lists the fitting parameters. Note that the amplitude of the sin contribution (c_0) is very small in most cases, for these we will only be interested in the $\langle A \rangle$ term. However in some cases the beating significantly interferes with the extraction of the material absorbance in the region of interest, and we will make use of the other parameters in these cases as will be detailed below. We will not try to obtained a sloped baseline correction as we did for CD shells in part because of the overtone at 5800 cm^{-1} and in part because in the case of CD shells the difference was relatively minor. We do note, however, that Figure A-14 does perhaps suggest a similar tilt, and also that the absorbance above 6000 cm^{-1} may be a little lower than in the 5250 to 4750 cm^{-1} region where we have obtained our baseline average. This may manifest itself in the zero thickness intercepts.

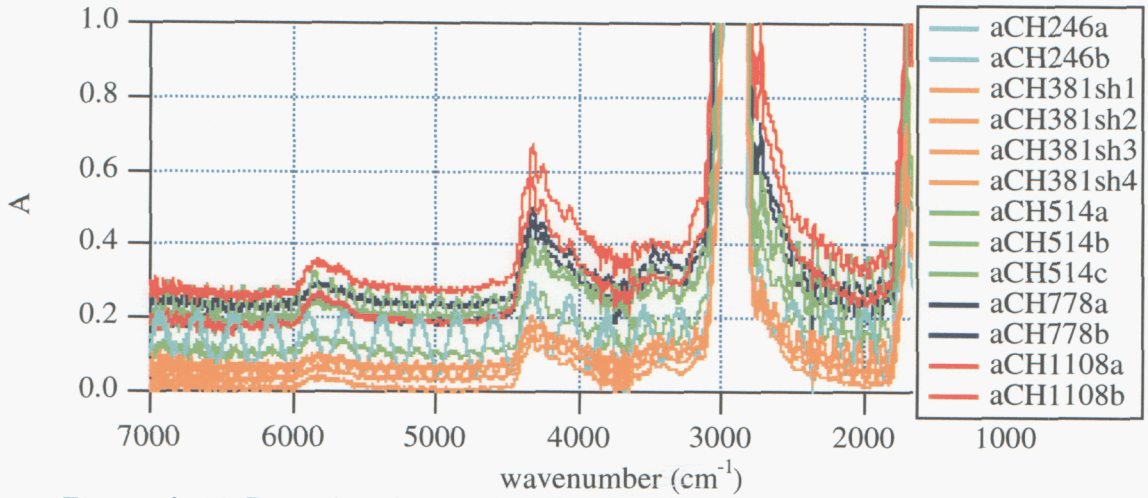

Figure A-14. Raw absorbance data for CH shells and shards.

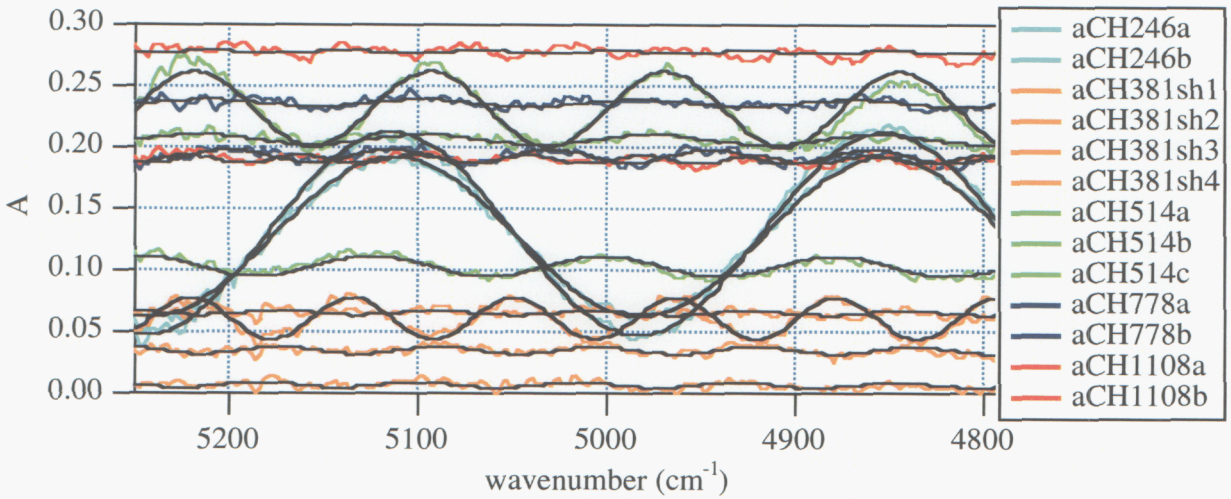

Figure A-15. Absorbance in the 5250 to 4750 cm^{-1} region with overlaid fits to eq A-2 in black.

Table A-II. Baseline correction fitting parameters (eq A-2).

sample	$\langle A \rangle$	c_0	c_1	c_2
CH246a	0.1271	0.06491	0.02418	3.603
CH246b	0.1297	0.08243	0.02402	4.402
CH381sh1	0.0607	0.01683	0.07334	1.968
CH381sh2	0.0068	-0.00208	0.07450	33.225
CH381sh3	0.0348	0.00295	0.07464	-26.418
CH381sh4	0.0651	0.00171	0.07569	-50.708
CH514a	0.2310	0.03071	0.05045	8.491
CH514b	0.1031	0.00830	0.05120	3.087
CH514c	0.2062	0.00406	0.05226	11.709
CH778a	0.2362	0.00273	0.05498	41.683
CH778b	0.1927	0.00549	0.07409	5.910
CH1108a	0.2777	0.00117	0.08729	-0.868
CH1108b	0.1900	0.00349	0.10410	-14.339

In Figure A-16 we show the absorbance in the region of interest corrected by the value of $\langle A \rangle$. There are several points to make. First, we need not worry about the absorbance in the region of the CH stretch at 2900 cm^{-1}, however the shoulders of this strong absorption may in part be affecting the other wavelengths of interest. Second, the baseline correction has brought together the multiple spectra from the same sample quite effectively. Third, for some of the spectra the thin film beating is clearly problematic. This is especially true of the CH246 data and certain of the CH381sh and CH514 data. It would be useful to be able to subtract out the contribution from this effect. For interference effects for light of wavelength λ traveling through a film of thickness t and refractive index n

$$m\lambda = 2t \times n \tag{A-3}$$

where m is an integer. Thus in terms of the wave number $\bar{\nu}$ the interval between successive ($\Delta m = 1$) beats depends only on the film thickness:

$$\frac{1}{\lambda} = \bar{\nu} = \frac{m}{2t \times n} \quad \Rightarrow \quad \Delta\bar{\nu} = \frac{1}{2t \times n} \quad . \tag{A-4}$$

This means that the constants c_1 and c_2 evaluated from the fits to eq A-2 should be valid throughout the wavenumber space. This is demonstrated in Figure A-17 for two sets of data where the fit is based *only* upon the data from 5250 to 4750 cm^{-1} but the fitted curves are extended down into the region of interest, only shifting them vertically. We see that the oscillation frequency of the fit (c_1) is the same, and even the phase lag (c_2) is not too bad given it was set 2000 wavenumbers away. However clearly the amplitude (c_0) of the oscillations has some wavenumber dependence as seen for the CH514a data. There are likewise amplitude variations for several of the other data sets.

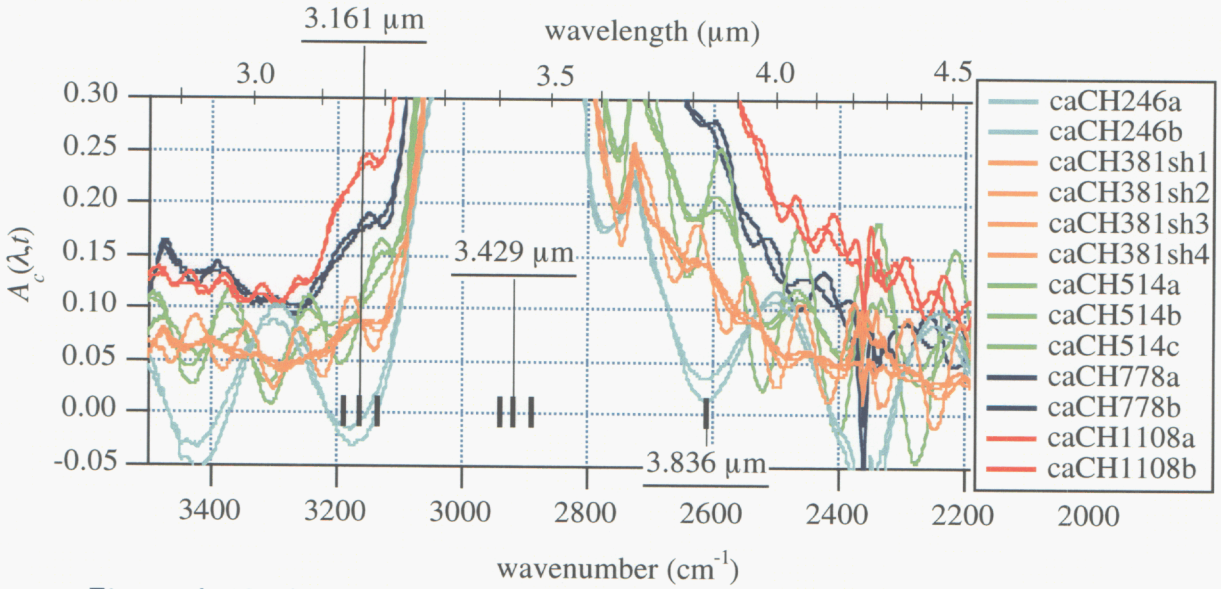

Figure A-16. Absorbances corrected by constant baseline correction $\langle A \rangle$.

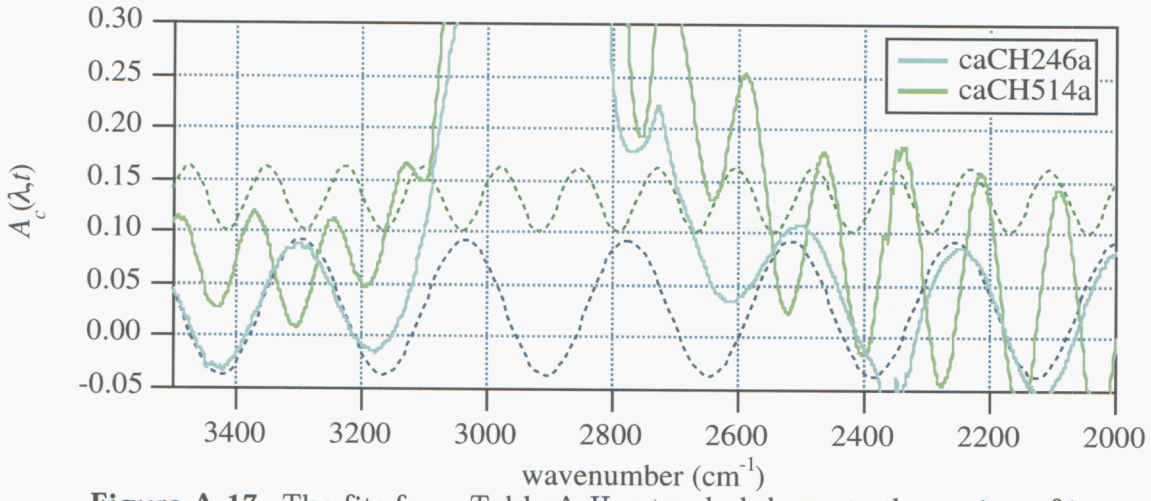

Figure A-17. The fits from Table A-II extended down to the region of interest demonstrating that the oscillation period of the fit (c_1) and phase lag (c_2) are reasonably wavenumber independent, while the amplitude (c_0) is not.

Our strategy will be to further correct the CH246 data sets where beating is especially significant in the region of interest by applying the sinusoidal fit (eq A-2 and Table A-II) using the values of c_1 and c_2 already determined and adjusting c_0 to match the amplitude of the beating in the region of interest. The results of doing this are shown in Figure A-18. Similar corrections to the other data sets that show beating were explored, but the variations in amplitude and the offset in phase made it difficult. Since the beating in these other cases is not so extreme, there are multiple data sets for each thickness and not all beat, and in general we have a lot of data, we will not pursue these corrections but rather deal with the scatter the beating may cause later.

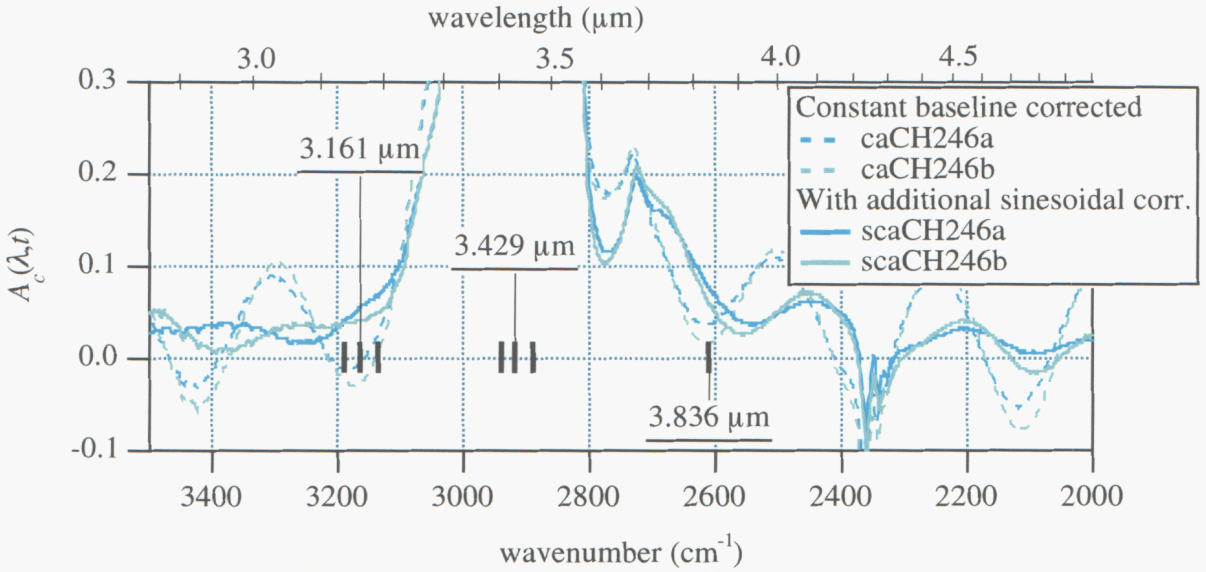

Figure A-18. Sinusoidal corrections to the CH246 data.

As we did with the CD data we will first look at simple thickness dependent corrected absorbance plots for the four wavelengths of interest, those around 3.2 and at 3.8 μm. The plot of this data is shown in Figure A-19. We see that the data is reasonably linear and at least for these four wavelengths give a near zero absorbance at the zero thickness intercept. The most serious scatter in the data is for the CH514 shell and as can be seen in Figure A-16 (and for one case in Figure A-17) this data had a fairly strong thin film oscillation perturbation. The effect on the extracted slope of the fitted lines is fairly minor, however, and we will not pursue a correction. In Figure A-20 we show the full set of fitted wavelength dependent extinction coefficients and in Figure A-21 the zero thickness intercepts. "Goodness" of fit $<r^2>$ values are shown in Figure A-22. In Table III in the main section we tabulate the extinction coefficients at the wavelengths of interest.

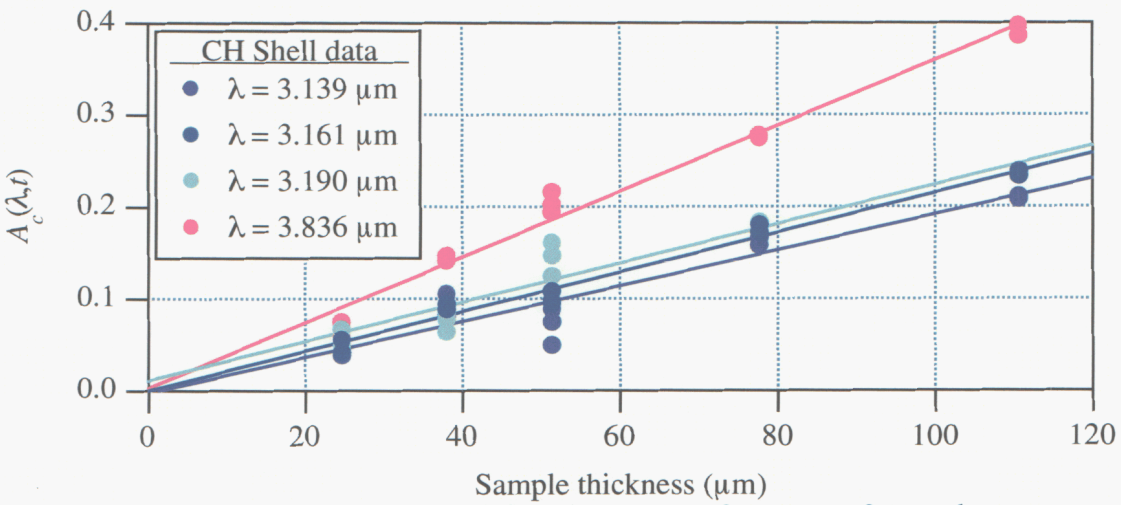

Figure A-19. Plot of corrected absorbance as a function of sample thickness for four wavelengths of interest.

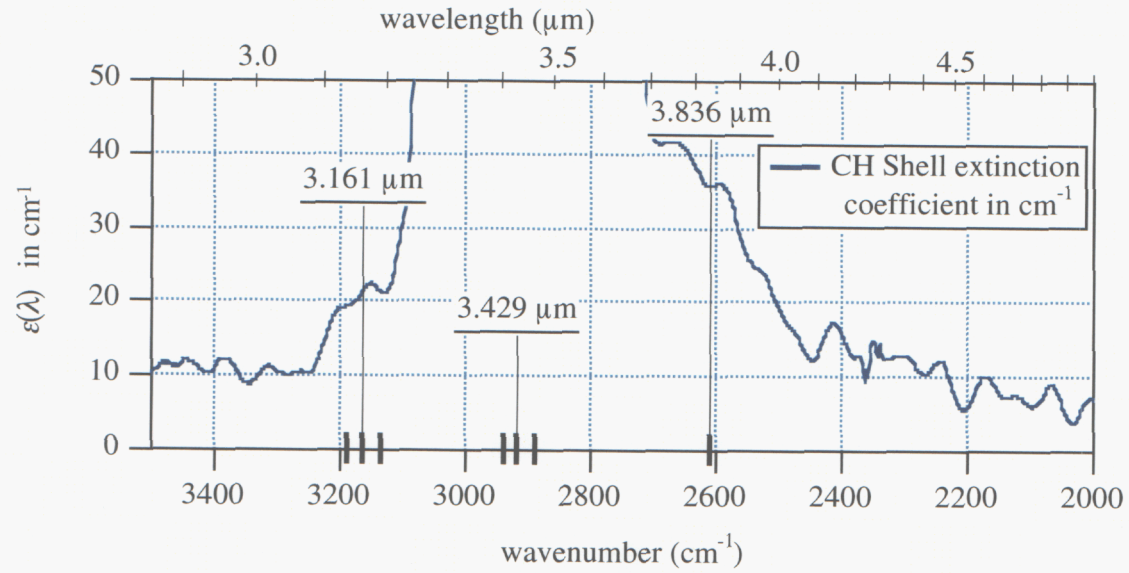

Figure A-20. CH shell extinction coefficient (cm^{-1}) as a function of wavenumber.

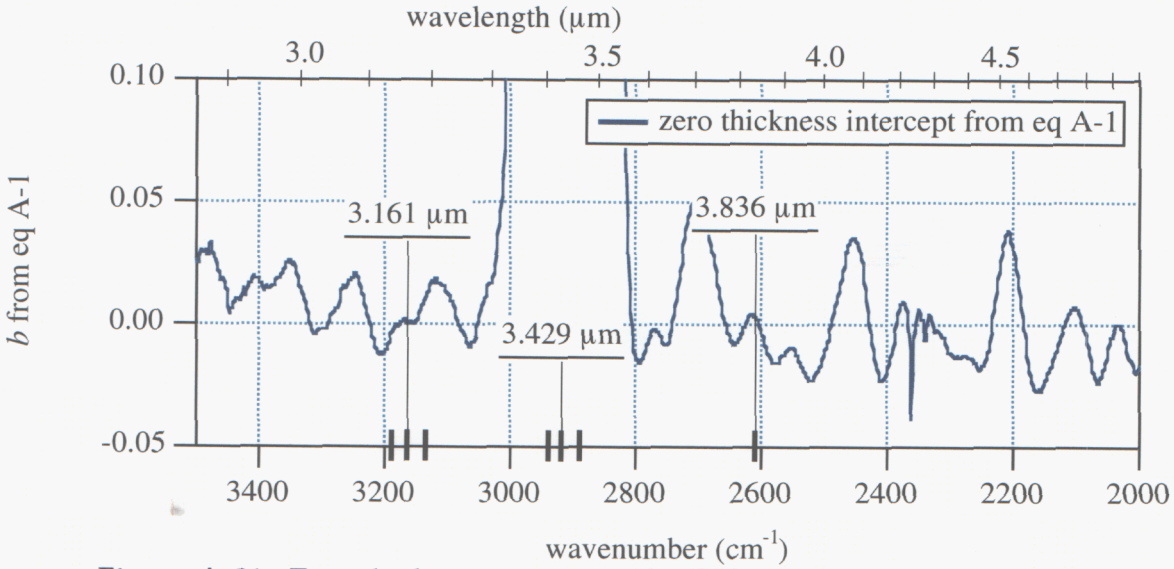

Figure A-21. Zero thickness intercepts for CH shell linear fits as a function of wave number

We see in Figure A-20 that the 3.2 and 3.8 μm wavelength regions sit on the shoulders of the huge CH stretch peak, and appear to be affected by it. The fits in both of these regions are good however, with near zero intercepts and $\langle r^2 \rangle$ greater than 0.9. The extracted values of $\varepsilon(\lambda)$ are larger by at least a factor of 2 from what was earlier reported for the 2-mm thin coating on a salt plate. The currently reported values for shells are certainly more representative of what can be expected. As a last item for this section we note that fits of this data around 3.4 μm gave nonsensical results because of saturation in transmission through even the thinnest samples.

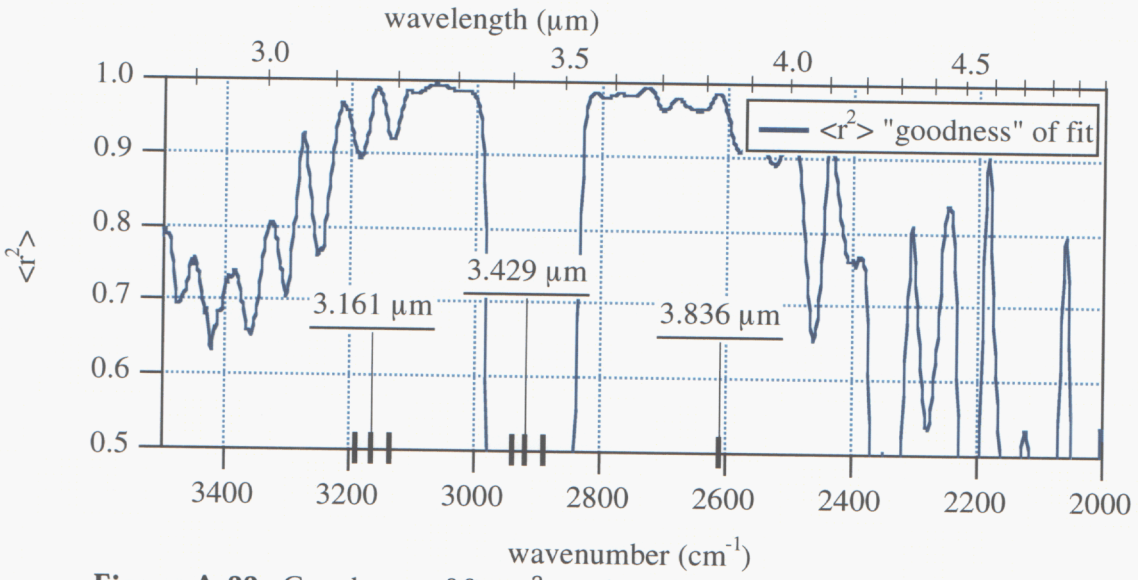

Figure A-22. Goodness of fit $<r^2>$ values for CH shell linear fit data.